International Journal of Applied Power Engineering (IJAPE)
Vol. 13, No. 3, September 2024, pp. 616~627
ISSN: 2252-8792, DOI: 10.11591/ijape.v13.i3.pp616-627

Coupled inductor interleaved boost converter with ANN and RNN based MPPT algorithm for PV system

K. S. Kavin[1], P. Subha Karuvelam[1], Naresh Kumar[2], Siddheswar Kar[3], Riyaz A. Rahiman[4], Sharda Patwa[3]

[1]Department of Electrical and Electronics Engineering, Government College of Engineering, Tirunelveli, India
[2]University Polytechnic, F/O Engineering and Technology, Jamia Millia Islamia Central University, New Delhi, India
[3]Department of Electrical Engineering, Medicaps University, Indore, India
[4]School of Electronics and Communication, Reva University, Bengaluru, India

Article Info

Article history:

Received Jul 27, 2023
Revised Feb 16, 2024
Accepted Mar 18, 2024

Keywords:

ANN-MPPT
Boost converter
Coupled inductor interleaved
EV
PV system
RNN based MPPT

ABSTRACT

An efficient machine learning approach for accomplishing the maximum power point tracking (MPPT) system for photovoltaic (PV) systems is proposed in this work. PV system is one of the most suitable renewable energy sources (RES) for electric vehicles (EV) based operations due to its ubiquitous availability and speed of installation. The deployment of PV-powered EVs reduces the quantity of carbon dioxide emitted into the atmosphere substantially. The primary objective of this research is to integrate a PV system with an EV load and to provide a constant power supply to the EV load with no distortions. A coupled inductor interleaved boost converter is used to raise voltage level of the PV because it has a wide conversions range with low leakage reaction times. Furthermore, the converter produces a consistent output with no fluctuations and high voltage gain. With the application of artificial neural network (ANN) based MPPT and recurrent neural network (RNN) based MPPT, the converter operational performance enhanced with steady dc link voltage is obtained. Consequently, it is stated that the employment of ANN and RNN-based MPPT controllers in PV-based systems offers improved DC link voltage regulation and lower power losses, thereby boosting system effectiveness. The MATLAB platform is used to test every component of the system's performance, and the findings show that the proposed system is more efficient than alternative approaches.

Corresponding Author:

K. S. Kavin
Department of Electrical and Electronics Engineering, Government College of Engineering
Tirunelveli, Tamil Nadu, India
Email: kavinksk@gmail.com

1. INTRODUCTION

Renewable energy sources (RES) are the most cost effective and pollutant free solution to offer renewable energy to all types of loads. Solar and wind energy are two of the most important RES on the entire planet. In general, solar energy is a preferred clean energy source due to its accessibility and encouraging nature for a wide range of power uses, especially electric vehicles (EV) and microgrid applications [1]–[4]. Considering its static construction, small size, and low maintenance cost, photovoltaic (PV) energy producing systems are frequently used. However, the voltage that is produced by the PV system is often low, which has an impact on system's effectiveness and dependability [5], [6]. Scientists use a variety of power electronic devices to address these difficulties, including inverters, voltage regulators, active power filters, and DC-DC converters [7]. Among these power electronic devices, DC-DC converters are particularly efficient for managing DC voltage and increasing an effectiveness of RES. Proper DC to DC converter design is a crucial factor that contributes significantly to the general efficiency of a system. The boost [8] converters is a common type converter that is used to enhance the resultant voltage of a PV panel, which offers a higher magnitude output voltage. However, boost converters have discontinuous input and output current, as well as significant output ripples. Buck-boost [9] converters can convert voltages in both directions, but their power output is limited by the discontinuous input current. Cuk [10] and single ended primary inductance converters (SEPIC) [11], [12], dealing with continuous input currents, eliminate these issues. These kinds of converters have incredibly huge current waves but perform voltages step-down and step-up. Furthermore, Cuk converters are confined to medium-low power uses and are susceptible to grid voltage variations. However, the SEPIC converter on the downside it faces the limitation of excessive current ripples. As a solution to the aforementioned issues, this article proposes coupled inductor interleaved boost converter. Due to the interleaved operation, the current ripples and leakage reactance are minimized, also it achieves a maximum voltage gain than other traditional converters.

Control strategies play critical roles in maximizing the power output of PV panels. Furthermore, the control strategies are used to optimize the overall functioning of converter topology. The most frequent ways for removing the optimal power from a PV system are perturb and observe [13]–[15] and incremental conductance [16]. These methods have particular drawbacks such as insecurity, complexity, challenges, and greater expense. To solve these problems, artificial intelligence (AI) technologies such as fuzzy logic controller (FLC) [17] and artificial neural network (ANN) [18], [19] have been developed. FLC has an efficient reaction, particularly in nonlinear control systems with ambiguous boundary conditions. FLC has several advantages, but it also has certain disadvantages, such as a longer calculating time, the need for rules for operation, and a longer settling time. ANN, on the other hand, is well-suited to dealing with nonlinear features of current voltage curves, but it requires a large amount of computation. Therefore, the RNN-based MPPT is used in this work for solving all of these issues. When contrasted to other MPPT controllers, it offers a fast-dynamic response and also it has robust performance.

Hence, this work implements the effective machine learning based MPPT method for delivering the constant power supply to the EV load with no distortions. With the addition of a coupled inductor interleaved boost converter, PV output voltage is further raised to the desired level. By utilization of ANN and RNN based MPPT approach, the maximal power from PV panels is observed with high efficiency. Compared to ANN-MPPT, the RNN gives better results with improved DC link voltage.

2. PROPOSED SYSTEM DESCRIPTION

Figure 1 represents the solar fed EV load with machine learning based control approach. Which contains the major elements including, PV system, coupled inductor interleaved DC-DC boost converter, ANN and RNN based MPPT controllers and EV load. Single PV panel produces a limited amount of electricity, necessitating the use of an enormous amount of PV panels. The coupled inductor interleaved boost converter avoids this situation. It is intended to boost PV output voltage while also efficiently minimizing steady-state error and producing a stabilized output. The oscillations in the converter output are balanced, and the converter produces a stable DC link voltage output with an aid MPPT controller. The desired PV voltage has been compared to the PV current of the solar system, and the expected error is then transmitted to an ANN and RNN based MPPT controller module. In this case, the RNN controller is superior to the ANN controller in terms of delivering improved control outputs. An efficient proposed control approach ensures stable power delivery to the EV load.

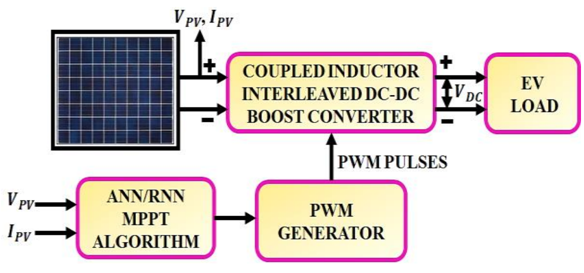

Figure 1. Proposed system

3. PROPOSED SYSTEM MODELLING

3.1. Modelling of PV system

In a solar energy system, several photovoltaic cells are linked in parallel and series to generate the required voltage or current. The diode that comprises up a PV cell and large p&n junction. A corresponding circuit for a single diode-based PV cell is shown in Figure 2. The formula for the solar cell output is as (1).

$$\mathrm{I_c} = \mathrm{I_{ph}} - \mathrm{I_0} = \mathrm{I_{ph}} - \mathrm{I_{sat}}\left[e^{\frac{q}{AKT_c}(V+IR_S)} - 1\right] \quad (1)$$

Where, the stack internal resistance, cell temperature, Boltzmann constant, and identity factor are all denoted by $K, R_S, T_c, and\ A$ correspondingly. $I_{sat}, I_{ph}, and\ q$, as well stands for the photocurrent, reverse saturation current of PN junctions and electron charge. The sufficient power for a solar energy system is generated by considering the series and parallel configurations of panels. Through the incorporation of an appropriate converter, the output obtained from the PV panel is significantly increased. In this research, an interleaved DC-DC converter is used, and it is described in the following manner.

3.2. Coupled inductor interleaved boost converter modelling

With the aid of a linked inductor interleaved boost converter, which generates high gain voltage with minimal leakage reactance, the achieved PV output is enhanced. Figure 3 depicts the equivalent circuit diagram of a connected inductor interleaved boost converter. The Figure 3 shows the coupled inductor's equivalent circuit while neglecting the winding resistance and core loss. L_m is mutual inductance, while T_m is a transformer with a turn ratio of 1. Leakage reactance in the primary winding and secondary winding are illustrated correspondingly by $L_1\ and\ L_2$. The currents entering into $L_1\ and\ L_2$ marked by $i_{L1}\ and\ i_{L2}$ can be represented as (2) and (3) using the identical circuit.

$$i_{L1} = i_{LM} + i_{T1} \quad (2)$$

$$i_{L2} = i_{T2} = -i_{T1} \quad (3)$$

Where by the transformer's main current, secondary current, and magnetic exciting current are designated as i_{T1}, i_{T1} and i_{LM} respectively. The input current shown by i_{in} in Figure 3 corresponds to the total of i_{L1} and i_{L2}. The magnetic departing current, i_{in} is equivalent to it according to (2) and (3). The equivalent circuit diagram of coupled inductor presented in Figure 4. The advantages of using coupled inductors in interleaved converters consist of increased system efficiency and reduced overall current ripples.

$$i_{in} = i_{L1} + i_{L2} = i_{LM} \quad (4)$$

The transformer's two separate windings have identical voltages; hence the equation can be written as (5).

$$v_T = \frac{L_M di_{LM}}{dt} \quad (5)$$

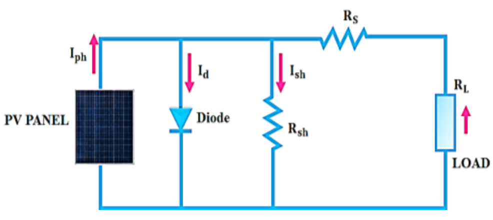

Figure 2. PV system model

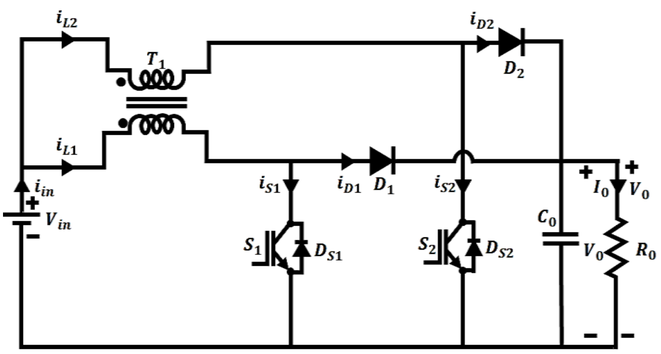

Figure 3. Proposed converter

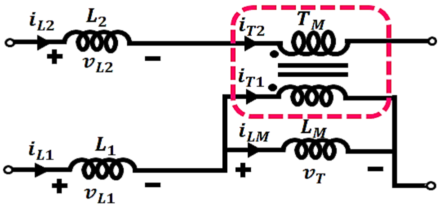

Figure 4. Coupled inductor equivalent circuit

3.2.1. Mode of operation

- Phase 1: ($\boldsymbol{t_0 < t < t_1}$)

Operating switches S_1 and S_2 have been switched on at the time of the start of phase 1. Two circuits of current are observed. One passes via S_1 and is i_{L1} and another one passes via S_2 and is i_{L2}. The majority of the magnetic stimulating i_{LM} are given by i_{L2} because S_2 gets turned on before S_1. In Figure 5(a), the comparable circuit is displayed. The secondary winding's parasitic capacitance C_{DS2} is where the current in the secondary winding i_{L2}. Switches from S_2. The voltage across C_{DS2} that is being charged takes relatively short time to reach the output voltage $V_O$since the parasitic capacitance is often extremely small**.** After that, C_{DS2} gets eliminated by i_{L2}, which instead flows via D_2 and the output capacitance C_O. The C_O is charged throughout this time. The following are the voltage computations for converter.

$$V_{in} = v_{L1} + v_T \tag{6}$$

$$V_{in} = v_{L2} + v_T + v_{DS2} = v_{L2} + v_T + V_0 \tag{7}$$

Where the voltages across leakage inductances $L1\ and\ L2$ are represented by the letters V_{L1} and V_{L2} correspondingly. The (6) and (7) combined result in (8) and (9).

$$2V_{in} = (v_{L1} + v_{L2}) + 2v_T + V_0 \tag{8}$$

The attained equation is derived from (8).

$$v_{L1} + v_{L2} = \frac{L_l di_{L1}}{dt} + \frac{L_l di_{L2}}{dt} + \frac{L_l di_{LM}}{dt} \tag{9}$$

Calculations (5) and (9) ought to be used as substitutes in (8) to determine the voltage across the mutual inductance.

$$v_T = \frac{L_M}{L_l + 2L_M}(2V_{in} - V_0) \tag{10}$$

Designing V_0 to be greater than twice V_{in} would result in an undesirable V_T and a linear reduction in i_{LM} in this mode. (12) can be used to represent the voltages across the leakage inductances by changing (6) and (7) to correspond to (10) accordingly.

$$v_{L1} = \frac{L_l V_{in}}{L_l + 2L_M} + \frac{L_M V_0}{L_l + 2L_M} \tag{11}$$

$$v_{L2} = \frac{L_l V_{in}}{L_l + 2L_M} - \frac{(L_l + L_M)V_0}{L_l + 2L_M} \tag{12}$$

Given that L_M is significantly bigger than L_1, (11) and (12) show that VL_1 is positive and VL_2 is negative. As a result, i_{L1} increases while i_{L2} declines linearly. It indicates a change in the direction of the magnetic stimulating current from the secondary winding to the primary winding.

- Phase 2: ($\boldsymbol{t_1 < t < t_2}$)

The switches both S_1 and S_2 are activated in this phase 2 mode and the diodes D_1 and D_2 are in OFF condition. Here, the voltages V_T, V_{L1} and V_{L2} are all positive. Hence, the i_{L1} and i_{L2} and i_{LM} are keep increasing. The voltage across the switch S_1 is becomes zero volts. S_1 is off condition and the circuits enter phase 3. The equivalent circuit of phase 2 is represented in Figure 5(b). The converter voltage equations are determined by neglecting diode conduction voltage.

$$V_{in} = v_{L1} + v_T \tag{13}$$

$$V_{in} = v_{L2} + v_T \tag{14}$$

Combining (13) and (14) produces (15).

$$2V_{in} = (v_{L1} + v_{L2}) + 2v_T \tag{15}$$

Substituting (5) and (9) into (15) results in (16).

$$v_T = \frac{2L_M V_{in}}{L_l + 2L_M} \tag{16}$$

When (17) is substituted for (13) and (14), the outcome is (17).

$$v_{L1} = v_{L2} = \frac{L_l V_{in}}{L_l + 2L_M} \tag{17}$$

v_T, v_{L1}, and v_{L2} are all positive in (16) and (17). Because the mutual inductance L_M is typically much more than leakage inductance L_1 the voltages v_{L1} and v_{L2} are relatively modest, and the currents i_{L2} and i_{L2} reach gradually.

- Phase 3: $(t_2 < t < t_3)$

Figure 5(c) depicts the corresponding circuitry of phase 3, with switch S_1 in the OFF position and S_2 in the ON position. C_{DS1} is the principal parasitic capacitance where the current in the primary winding i_{L1} changes from S_1. Because the parasitic capacitance is generally very low, the voltage across C_{DS1} that is getting charged requires a remarkably quick period to attain the output voltage V_O. Following that C_{DS1} is removed by i_{L1}, which instead flows through D_1 and the output capacitance C_O. The voltage equations of phase 3 is similar to the phase 1 and 2. The suggested converter employs an ANN and RNN based MPPT controller, which is primarily employed for optimum control and observes PV system's maximum power respectively.

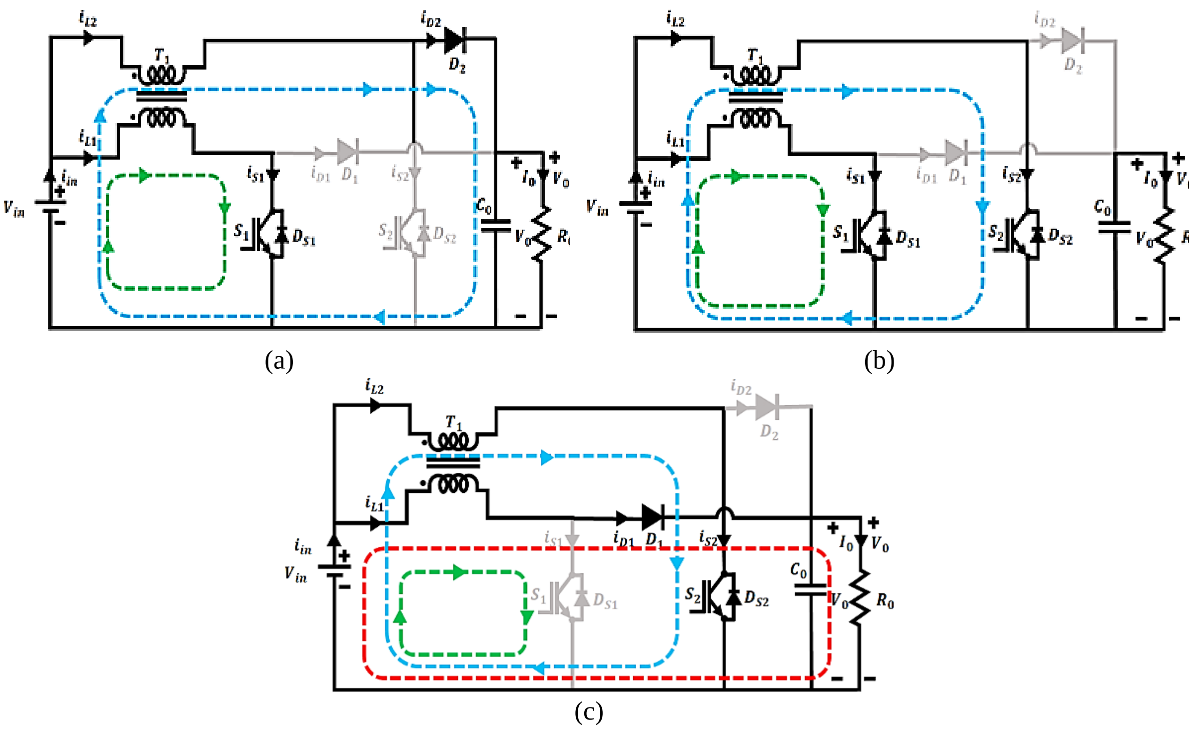

Figure 5. Modes of operation 5 (a) phase 1, (b) phase 2, and (c) phase 3

3.3. ANN based MPPT

A type of artificial intelligence technique is the ANN. The use of artificial intelligence has more benefits than traditional methods. The general structure of ANN in MPPT is shown in Figure 6. Solar temperature and irradiance are the inputs. The NN intended goal is to reduce duty ratio of the proposed DC to DC converter. A specific value of duty ratio is provided by the neural network for each variation in solar temperature and irradiance in order to obtain the greatest power point.

Levenberg-Marquardt algorithmic training method is used to build the network. Duty factor is obtained and ANN is trained for different solar irradiance and temperature value combinations. To get the desired values, the weights of layers need to be adjusted throughout neural network training. To monitor target values with the least amount of error, weights are changed during training. MSE is the ANN's effectiveness measurement. If an is the current output and t is the target, the attained MSE as in (18).

$$F = \frac{1}{N}\sum_{i=1}^{N}(t_i - a_i)^2 \tag{18}$$

The ANN provides additional advantages such as quick response times for optimal power point tracking, lower steady state error, and no need for reprogramming because the learning mechanism is built-in. Although the neural network framework is having a complex design, it requires intensive training. These issues tackled by using RNN based MPPT algorithm and the following section gives a detailed description of RNN-MPPT controller.

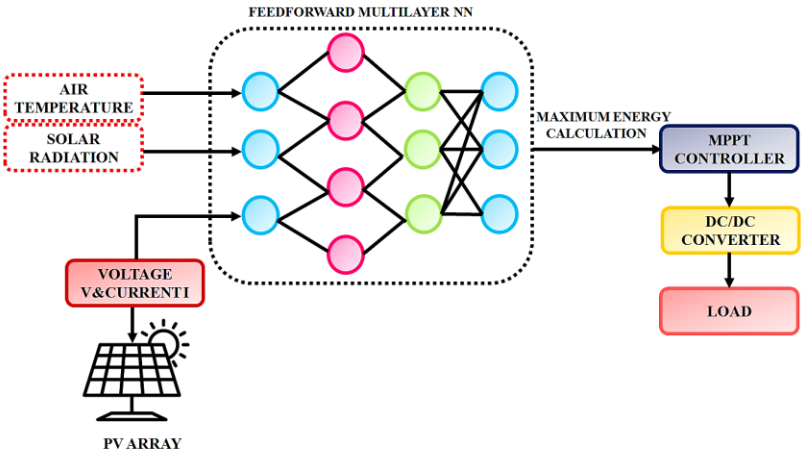

Figure 6. Structure of ANN based MPPT

3.4. RNN based MPPT

RNN belongs to a type of ANN which employs data from earlier iterations to enlarge the accuracy of network on inputs from the present and the future. Since RNNs are the only networks that have loops and a concealed state (memory), they are frequently regarded to be exceptional when compared to other networks. The RNN is able to function on sequences and store previous knowledge in the hidden state according to its structure. To put it another way, it receives a portion of its output as input for the following time step. These characteristics make it possible to solve a variety of issues involving sequential data of various lengths. Many RNN designs have been introduced in recent years, includes fully recurrent (FRNN), gated recurrent units (GRUs), and long short-term memory (LSTM). RNN setup was utilized in various filtering and modelling applications due to its low complexity. (19) and (20) is used to define the hidden layer and the RNN output.

$$h_t = \sigma_h(W_h x_t + U_h h_{t-1} + b_h) \tag{19}$$

$$y_t = \sigma_y\left(W_y h_t + b_y\right) \tag{20}$$

Where x_t, h_t, and y_t are the input, hidden layer and output vectors, correspondingly; $W, U, and\ b$ are variable matrices and vectors; and h and y are the corresponding activation function, provided in (21) and (22) accordingly.

$$\sigma_h(x) = \frac{2}{1+e^{-2x}} - 1 \tag{21}$$

$$\sigma_y(x) = x \tag{22}$$

This work chooses temperature and irradiation as two input feature vectors to train the RNN model, and output is the reference current vector I_{mpp} that reflects MPP's continuous operation. The dataset utilized in this study contains normalized samples, 15% of which were used for validation and 15% for testing. The error is the variation among the expected result target, and N is the quantity of training data. MSE, which is specified in (23), is used to calculate the training performance.

$$MSE = \frac{1}{N}\sum_{i=0}^{N}(e_i)^2 \quad (23)$$

Figure 7 illustrates the architecture for RNN based MPPT controller for PV system. When compared ANN–MPPT, it attains high prediction output results with stabilized DC output voltage. It is also observing the optimal power from PV within a short period.

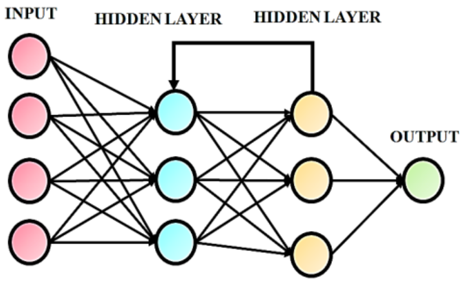

Figure 7. Structure of RNN based MPPT

4. RESULTS AND DISCUSSION

For the purpose of offer a consistent power supply to the EV load without any interruptions, this research incorporates a reliable machine learning-based MPPT approach. The consideration of a linked inductor interleaved boost converter raises the PV output voltage to appropriate level. The greatest amount of energy from PV panels is observed with outstanding efficiency by using an ANN and RNN based MPPT technique. The RNN performs better than ANN-MPPT and has superior DC link voltage. In MATLAB/Simulink, the entire validation of the suggested approach is carried out. The parameter requirements of the proposed systems are presented in Table 1.

Table 1. Parameter description

Parameter	Specification
Solar PV system	
Series connected solar PV cells	36
Short circuit current	8.33 A
Open circuit voltage	12 V
Peak power	10 KW, 10 panels
Coupled inductor interleaved boost converter	
Winding 1 self-impedance	
$L_1(H)$	1.1 mH
$R_1(ohm)$	1.1
Winding 2 self-impedance	
$L_1(H)$	1.1 mH
$R_1(ohm)$	1.1

4.1. At variation of temperature and intensity

A temperature change is introduced after 0.2 sec as indicated in Figure 8 to evaluate the efficiency of the suggested strategy in addressing an intermittent nature of the PV system. Temperature unexpectedly rises from 25°C to 35°C at this same moment. There is a similar variation in solar irradiation from 800 W/Sq. to 1000 W/Sq. as there is in temperature. The PV voltage maintains the constant voltage 120 V after 0.2 sec and current becomes stable value of 15 Amps after 0.23 sec.

Figure 9 representing the waveforms for output voltage and current of coupled inductor interleaved boost converter using MPPT control method. Here, by the employment of ANN and RNN based MPPT approach, the constant output voltage 330 V is obtained, after 0.2 seconds as seen in Figures 9(a) and 9(b) respectively. Likewise, the Figure 9(c) represents constant current 5 Amps is attained.

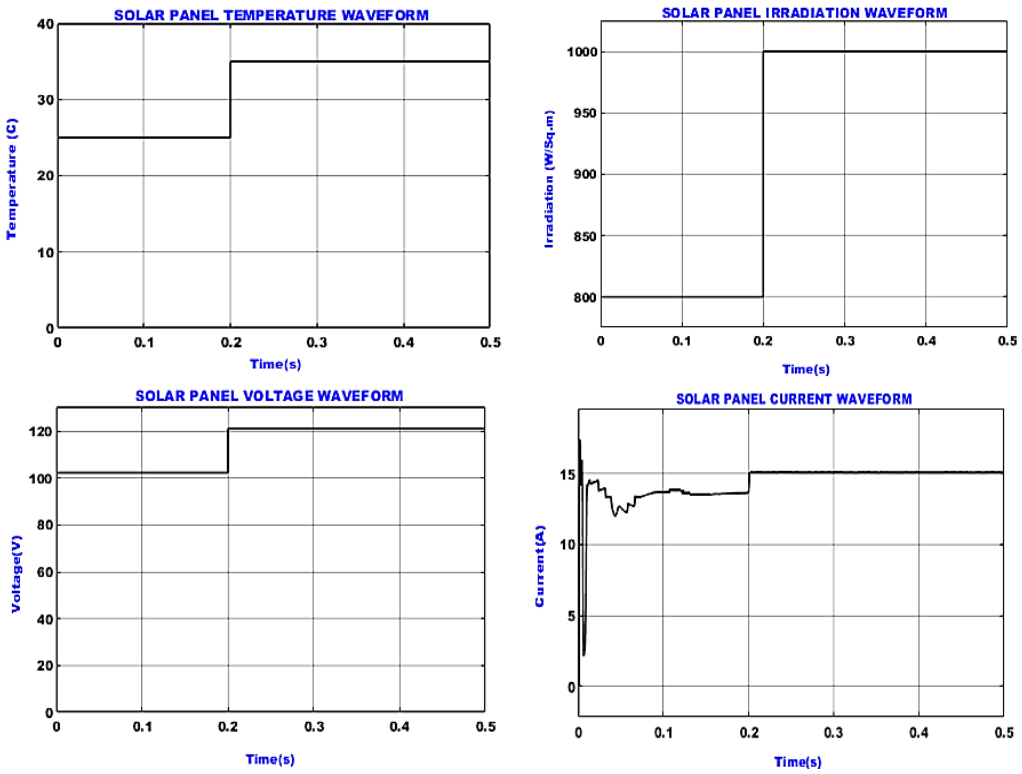

Figure 8. At variation of parameter PV panel

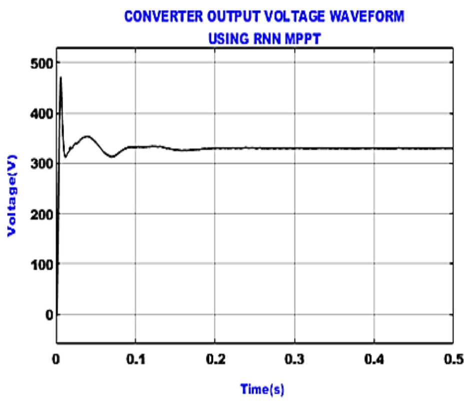

(a)

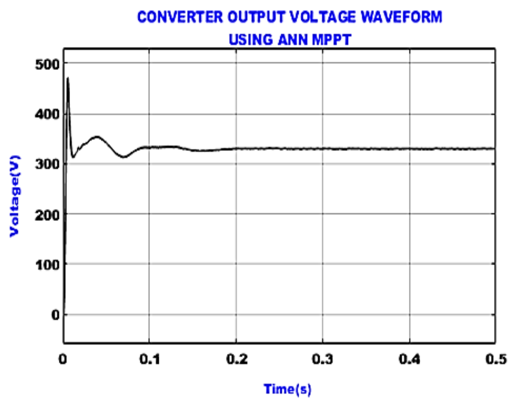

(b)

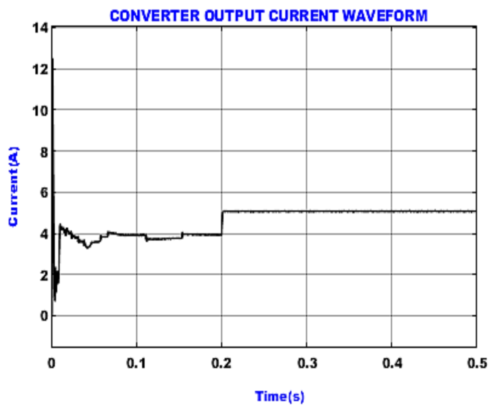

(c)

Figure 9. Waveforms representing the output voltage of converter using (a) ANN based MPPT, (b) RNN based MPPT, and (c) output current

4.2. At constant temperature and intensity

The Figure 10 illustrates PV system parameters comprising temperature, irradiation, voltage and current. A constant temperature and irradiation value of 35 °C and 1000 W/Sq is attained respectively. Similarly, the steady voltage 120 V is obtained and the current takes 0.13 sec to maintain the constant value of 15 Amps.

Figure 11 displays the output voltage and current waveforms of a proposed converter that uses the MPPT control technique. A fixed output voltage 330 V is reached after 0.2 sec by employing an ANN and RNN based MPPT technique, as shown in Figures 11(a) and 11(b). Similarly, Figure 11(c) shows that a steady current of 5 Amps is obtained. Table 2 indicates the comparison analysis of suggested converter with another various converter such as boost [18], Cuk [19], SEPIC [20], and Luo [21]. The attained outcomes show that the proposed has high efficiency 95% compared other approaches, that is depicted in Figure 12. Table 3 denotes the attained tracking efficiency of different MPPT controller with recommended controllers. Figure 13 clearly illustrates that the RNN based MPPT achieves the highest tracking efficiency value of 98.3% when compared to other methods.

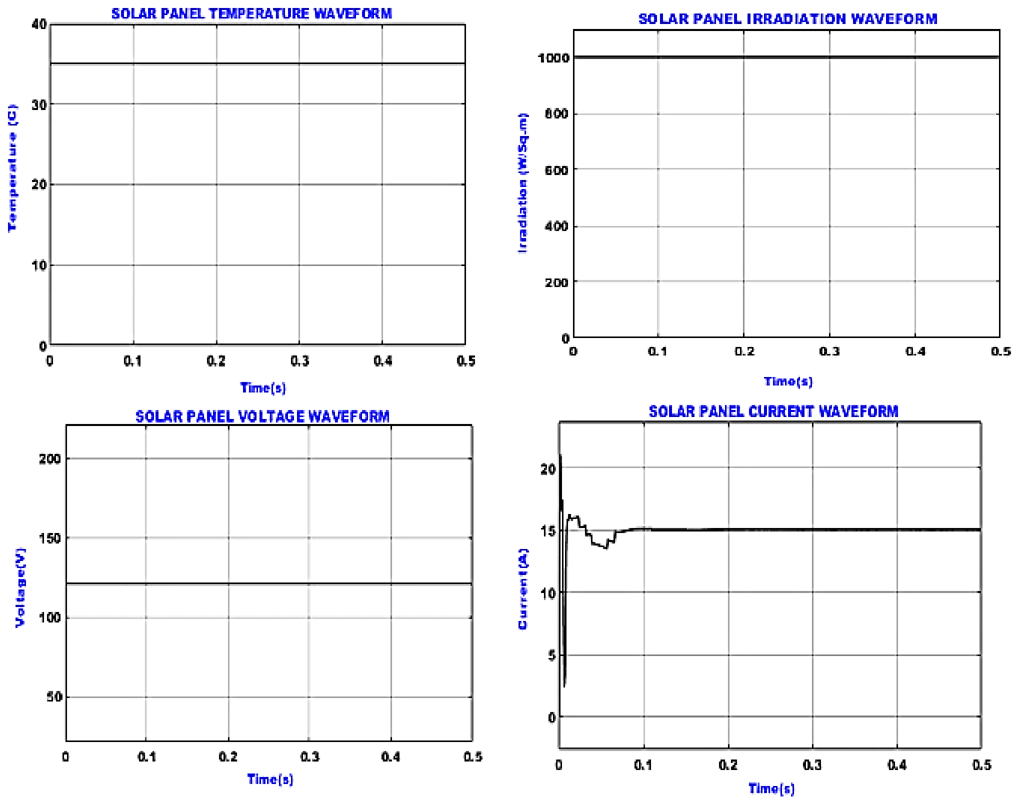

Figure 10. Parameters of PV panel

Table 2. Comparison analysis of converters efficiency

Converters	Efficiency (%)
Boost	80 [20]
Cuk	85 [21]
SEPIC	88.82 [22]
Luo	90 [23]
Coupled inductor interleaved boost	95%

Table 3. Comparison analysis of MPPT controllers tracking efficiency

Mppt methods	Tracking efficiency (η_{MPPT}%)
PI based P&O [24]	95%
IncCond [25]	96.8%
ANN-MPPT	97.2%
RNN-MPPT	98.3%

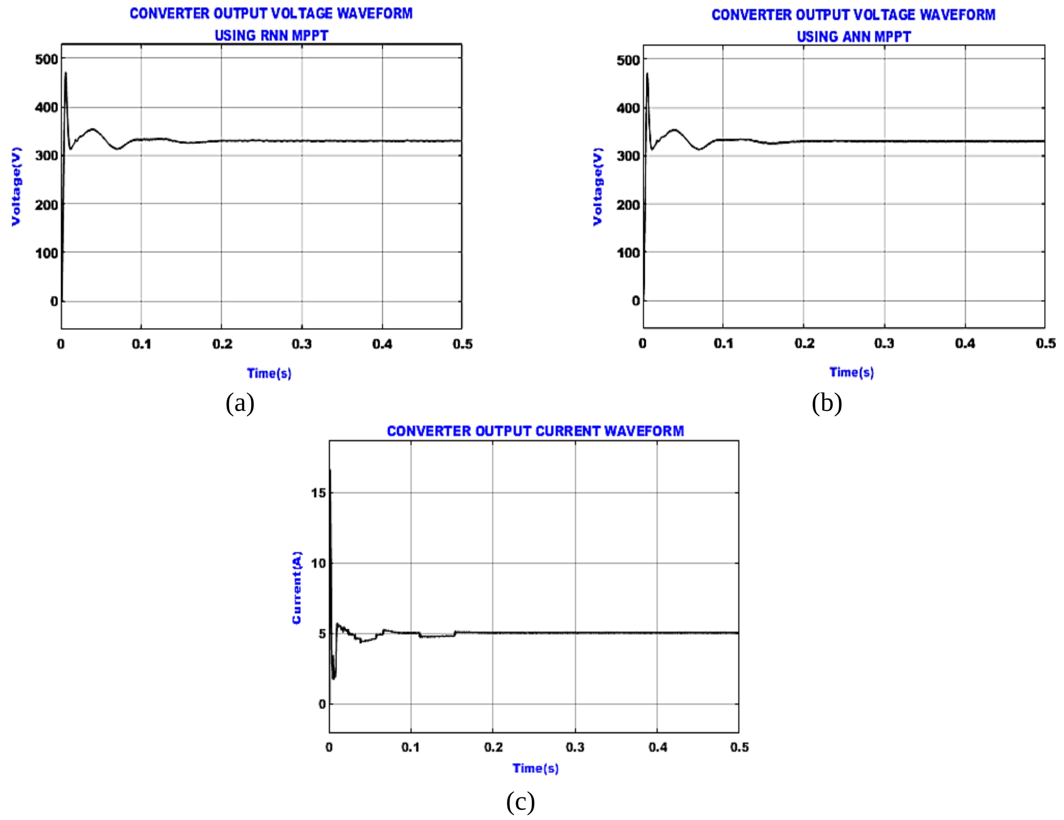

Figure 11. Waveforms demonstrating the output voltage of converter using (a) ANN based MPPT, (b) RNN based MPPT, and (c) output current

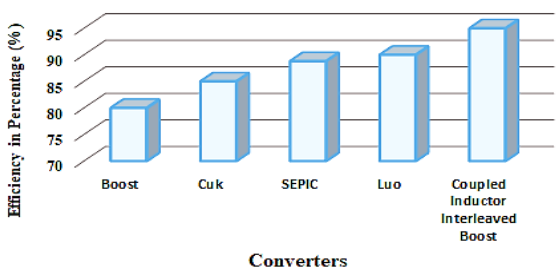

Figure 12. Comparison analysis of efficiency

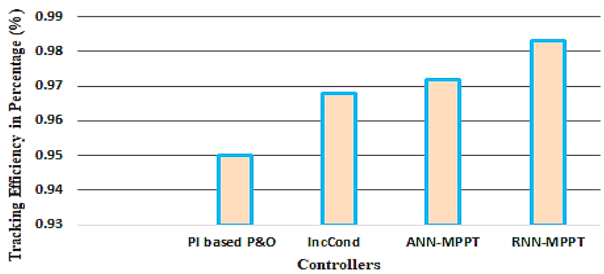

Figure 13. Comparison analysis of tracking efficiency

5. CONCLUSION

The purpose of the research is to combine a PV system with an EV load and deliver a consistent power supply to the EV load. To boost a voltage level of the PV, a coupled inductor interleaved boost converter is used because it offers a wide conversion range and low leakage reactance. In addition, the converter generates a stable output with no fluctuations and a high voltage gain. The implementation of ANN-based MPPT and RNN-based MPPT results in improved converter operational efficiency with constant dc link voltage. As a result, it has been suggested that using ANN and RNN-based MPPT controllers in PV-based systems provides enhanced DC link voltage management and decreased power losses with increasing system efficacy is attained. Hence, it is concluded that the proposed system obtains highest converter efficiency 95% and tracking efficiency 98.3% respectively. The proposed system is more efficient than other existing techniques, according to the results.

REFERENCES

[1] K. S. Kavin, P. S. Karuvelam, A. Pathak, T. R. Premila, R. Hemalatha, and T. Kumar, "Modelling and analysis of hybrid fuzzy tuned PI controller based PMBLDC motor for electric vehicle applications," *International Journal of Electrical and Electronics Engineering*, vol. 10, no. 2, pp. 8–18, Feb. 2023, doi: 10.14445/23488379/IJEEE-V10I2P102.

[2] K. S. Kavin and P. S. Karuvelam, "PV-based grid interactive PMBLDC electric vehicle with high gain interleaved DC-DC SEPIC converter," *IETE Journal of Research*, vol. 69, no. 7, pp. 4791–4805, Sep. 2023, doi: 10.1080/03772063.2021.1958070.
[3] D. Akinyele, J. Belikov, and Y. Levron, "Battery storage technologies for electrical applications: Impact in stand-alone photovoltaic systems," *Energies*, vol. 10, no. 11, p. 1760, Nov. 2017, doi: 10.3390/en10111760.
[4] K. M. S. Y. Konara, M. L. Kolhe, and A. Sharma, "Power dispatching techniques as a finite state machine for a standalone photovoltaic system with a hybrid energy storage," *AIMS Energy*, vol. 8, no. 2, pp. 214–230, 2020, doi: 10.3934/energy.2020.2.214.
[5] K.-S. Ryu *et al.*, "MPC based energy management system for hosting capacity of PVs and customer load with ev in stand-alone microgrids," *Energies*, vol. 14, no. 13, p. 4041, Jul. 2021, doi: 10.3390/en14134041.
[6] M. Babaei, E. Azizi, M. T. Beheshti, and M. Hadian, "Data-Driven load management of stand-alone residential buildings including renewable resources, energy storage system, and electric vehicle," *Journal of Energy Storage*, vol. 28, p. 101221, Apr. 2020, doi: 10.1016/j.est.2020.101221.
[7] D. G and S. N. Singh, "Selection of non-isolated DC-DC converters for solar photovoltaic system," *Renewable and Sustainable Energy Reviews*, vol. 76, pp. 1230–1247, Sep. 2017, doi: 10.1016/j.rser.2017.03.130.
[8] M. I. S. Guerra, F. M. Ugulino de Araújo, M. Dhimish, and R. G. Vieira, "Assessing maximum power point tracking intelligent techniques on a PV system with a buck–boost converter," *Energies*, vol. 14, no. 22, p. 7453, Nov. 2021, doi: 10.3390/en14227453.
[9] T. Rahimi, M. R. Islam, H. Gholizadeh, S. Mahdizadeh, and E. Afjei, "Design and implementation of a high step-up DC-DC converter based on the conventional boost and buck-boost converters with high value of the efficiency suitable for renewable application," *Sustainability*, vol. 13, no. 19, p. 10699, Sep. 2021, doi: 10.3390/su131910699.
[10] Z. Sun and Z. Yang, "Improved maximum power point tracking algorithm with cuk converter for PV systems," *The Journal of Engineering*, vol. 2017, no. 13, pp. 1676–1681, Jan. 2017, doi: 10.1049/joe.2017.0617.
[11] A. Kasasbeh, B. Kelleci, S. B. Ozturk, A. Aksoz, and O. Hegazy, "SEPIC converter with an LC regenerative Snubber for EV applications," *Energies*, vol. 13, no. 21, p. 5765, Nov. 2020, doi: 10.3390/en13215765.
[12] V. Kumar, S. Ghosh, N. K. S. Naidu, S. Kamal, R. K. Saket, and S. K. Nagar, "A current sensor based adaptive step-size MPPT with SEPIC converter for photovoltaic systems," *IET Renewable Power Generation*, vol. 15, no. 5, pp. 1085–1099, Apr. 2021, doi: 10.1049/rpg2.12091.
[13] A. Chellakhi, S. El Beid, and Y. Abouelmahjoub, "An improved adaptable step-size P&O MPPT approach for standalone photovoltaic systems with battery station," *Simulation Modelling Practice and Theory*, vol. 121, p. 102655, Dec. 2022, doi: 10.1016/j.simpat.2022.102655.
[14] R. John, S. S. Mohammed, and R. Zachariah, "Variable step size Perturb and observe MPPT algorithm for standalone solar photovoltaic system," in *2017 IEEE International Conference on Intelligent Techniques in Control, Optimization and Signal Processing (INCOS)*, Mar. 2017, pp. 1–6. doi: 10.1109/ITCOSP.2017.8303163.
[15] S. K. Ramu *et al.*, "A novel high-efficiency multiple output single input step-up converter with integration of Luo network for electric vehicle applications," *International Transactions on Electrical Energy Systems*, vol. 2022, pp. 1–13, Sep. 2022, doi: 10.1155/2022/2880240.
[16] Patnaik and T. Anuradha, "Adaptive incremental-conductance MPPT based solar PV system for electric vehicles," *Journal of Electrical Engineering*, vol. 18, no. 4, p. 10, 2018.
[17] N. Priyadarshi, V. Ramachandaramurthy, S. Padmanaban, and F. Azam, "An Ant Colony optimized MPPT for standalone hybrid PV-wind power system with single Cuk converter," *Energies*, vol. 12, no. 1, p. 167, Jan. 2019, doi: 10.3390/en12010167.
[18] S. R. Kiran, C. H. H. Basha, V. P. Singh, C. Dhanamjayulu, B. R. Prusty, and B. Khan, "Reduced simulative performance analysis of variable step size ANN based MPPT techniques for partially shaded solar PV systems," *IEEE Access*, vol. 10, pp. 48875–48889, 2022, doi: 10.1109/ACCESS.2022.3172322.
[19] B. Cortés, R. Tapia, and J. J. Flores, "System-independent irradiance sensorless ANN-Based MPPT for photovoltaic systems in electric vehicles," *Energies*, vol. 14, no. 16, p. 4820, Aug. 2021, doi: 10.3390/en14164820.
[20] F. Nejabatkhah, S. Danyali, S. H. Hosseini, M. Sabahi, and S. M. Niapour, "Modeling and control of a new three-input DC–DC boost converter for hybrid PV/FC/battery power system," *IEEE Transactions on Power Electronics*, vol. 27, no. 5, pp. 2309–2324, May 2012, doi: 10.1109/TPEL.2011.2172465.
[21] F. Galea, M. Apap, C. Spiteri Staines, and J. Cilia, "Design of a high efficiency wide input range isolated Cuk Dc-Dc converter for grid connected regenerative active loads," in *World of EngineerinG Convention*, 2011, pp. 1–11.
[22] P. Javeed, L. K. Yadav, P. Venkatesh Kumar, R. Kumar, and S. Swaroop, "SEPIC converter for low power LED applications," *Journal of Physics: Conference Series*, vol. 1818, no. 1, p. 012220, Mar. 2021, doi: 10.1088/1742-6596/1818/1/012220.
[23] S. Sivarajeswari and D. Kirubakaran, "RETRACTED: Design and development of efficient Luo converters for DC micro grid," *International Journal of Electrical Engineering & Education*, vol. 60, no. 1_suppl, pp. 1662–1682, Oct. 2023, doi: 10.1177/0020720919845152.
[24] D. Sera, L. Mathe, T. Kerekes, S. V. Spataru, and R. Teodorescu, "On the perturb-and-observe and incremental conductance MPPT methods for PV systems," *IEEE Journal of Photovoltaics*, vol. 3, no. 3, pp. 1070–1078, Jul. 2013, doi: 10.1109/JPHOTOV.2013.2261118.
[25] G.-C. Hsieh, H.-I. Hsieh, C.-Y. Tsai, and C.-H. Wang, "Photovoltaic power-increment-aided incremental-conductance MPPT with two-phased tracking," *IEEE Transactions on Power Electronics*, vol. 28, no. 6, pp. 2895–2911, Jun. 2013, doi: 10.1109/TPEL.2012.2227279.

BIOGRAPHIES OF AUTHORS

K. S. Kavin received his Electrical and Electronics Engineering degree from CSI Institute of Technology, Nagercoil, India, in 2009 from Anna University; and his Master's degree in Power Electronics and Drives from Anna University (Shanmuganathan Engineering College, Pudukkottai), India, in 2014. Presently, he is pursuing his full-time Ph.D. degree in Anna University, Chennai, India. His current research interests include BLDC motors, shunt active filter, and DC-DC converters. He can be contacted at email: kavinksk@gmail.com.

P. Subha Karuvelam received Electrical and Electronics Engineering degree from PSG College of technology, Coimbatore and Master's degree in Power Electronics and Drives from Government College of Engineering, Tirunelveli, India, in 1996 and 2005, respectively. She completed Ph.D. in Electrical Engineering from Anna University, Chennai, India, in 2015. From 2001, she started working as assistant professor in the Department of Electrical and Electronics Engineering, Government College of Engineering, Tirunelveli. In 2019, she was promoted associate professor in Government College of Engineering, Tirunelveli. Her current research interests are intelligent control techniques, power quality monitoring, power electronic converters, and AC drives. She has published more than 20 research articles in national and international journals. She can be contacted at email: subha@gcetly.ac.in.

Naresh Kumar received his Bachelor Degree in Electrical Engineering in 2001 and Master of Technology in Power System in 2005 from Central University Jamia Millia Islamia, New Delhi, India and pursuing Ph.D. from the same university. Presently, he is working as assistant professor in the University Polytechnic, F/O Engineering and Technology, Jamia Millia Islamia Central University, New Delhi. His research interests include electrical power systems, renewable energy, and electrical machines/drives. He can be contacted at email: nkumar2@jmi.ac.in.

Siddheswar Kar working as an assistant professor in the Department of Electrical Engineering at Medi-Caps University, Indore, MP, India. He obtained B.E. Degree in Electrical Engineering from Orissa Engineering College, Bhubaneswar, Orissa, India in 2000. He received M.Tech. degree in Power Control and Drives specialization from NIT Rourkela, Odisha, India in 2010. He is pursuing his Ph.D. in Electrical Engineering from Biju Patnaik University of Technology, Odisha, India. He has more than 20 years of teaching experience. He has published papers in various national, international journals, and conferences. He has published patents and books. His current research areas of interest are power electronics, electrical drives, and renewable energy systems. He can be contacted at email: siddheshwar.kar@medicaps.ac.in.

Riyaz A. Rahiman received the Bachelor's Degree in Electronics and Communication Engineering, in 2006, from Mahatma Gandhi University, Kottayam, Kerala (India) and Master of Technology in Control and Instrumentation in 2013 from Anna University Chennai, India and Ph.D. in Electrical and Electronics from the Bharath University, Chennai, India. Presently he is working as associate professor with the School of Electronics and Communication at REVA University, Bangalore, Karnataka, India. His current research interests include power electronics, electric motor control systems, renewable energy systems, and autonomous control. He can be contacted at email: riyaz.arahiman@reva.edu.in.

Sharda Patwa received her Bachelor Degree in Electrical Engineering in 2010 and Master of Engineering in Control System Engineering in 2012 from Jabalpur Engineering College Jabalpur Madhyapradesh, India, and pursuing Ph.D. from the Medi-caps University. Presently, she is working as assistant professor in the Medi-caps University Indore Madhya Pradesh. Her research interests include electrical power systems, renewable energy, and electrical machines/drives. She can be contacted at email: sharda.patwa@medicaps.ac.in.